ELSEVIER

Chemical Engineering Science 59 (2004) 5687–5694

Chemical Engineering Science

www.elsevier.com/locate/ces

Production of sodium bicarbonate in industrial bubble columns

Benoît Haut[a,*], Véronique Halloin[a], Thierry Cartage[b], Arnaud Cockx[c]

[a]*Applied Science, Chemical Engineering, Université Libre de Bruxelles, 50 av. F.D. Roosevelt, CP 165/67, 1050 Brussels, Belgium*
[b]*Solvay SA, Direction Process Engineering, rue de Ransbeek 310, 1120 Brussels, Belgium*
[c]*INSA, Département G.P.I., 135 av. de Rangueil, 31077 Toulouse Cedex 4, France*

Received 27 February 2004; received in revised form 29 June 2004; accepted 27 July 2004
Available online 1 October 2004

Abstract

Industrial production of refined sodium bicarbonate proceeds in large-scale bubble columns. The main purpose of the research is to develop a mathematical model for a specific column. In order to characterize the column, several types of measurements (performed at different scales) are presented and analyzed. Consequently, a 1D model of the column is constructed including two bubble populations. Closure of the model is done using Computational Fluid Dynamics and experimental data collected on the industrial column. A model of gas–liquid mass transfer is also developed.

Keywords: Hydrodynamics; Bubble columns; Gammametric measurements; Particle image velocimetry

1. Introduction

This work is part of a research project between Solvay S.A. and the Brussels University. Aim of this project is to understand the physical and chemical behaviors of bubble columns involving a precipitation reaction of refined sodium bicarbonate ($NaHCO_3$). The complexity of the problem lies in the coupling between several complex phenomena met in these reactors (three-phase flow, enhanced CO_2 mass transfer, precipitation, ...).

The main purpose of this work is to develop a model for an industrial column, located in Dombasle (France), used for the precipitation of refined sodium bicarbonate. The 20 m high and 2.5 m wide nearly isothermal column is composed of a cylindrical core equipped with trays in its upper part (Fig. 1). These trays limit liquid back mixing and therefore increase gas–liquid mass transfer. In the lower part of the column, two circulation loops are found. In Fig. 1, a coordinate z is introduced. $z = 0$ at the bottom of the column; $z = z_1$ at the top of the circulation loops and $z = z_2$ at the bottom of the tray region.

The column is fed at the top with a liquid mixture composed mainly of the following chemical species: H_2O, $HCO3^-$, CO_3^{2-} and Na^+. A mixture of air and CO_2 is injected at its bottom. The following reactions take place in the column:

$$CO_{2,(g)} \rightleftharpoons CO_{2,(l)}, \tag{1}$$

$$CO_{2,(l)} + OH^- \rightleftharpoons HCO_3^-, \tag{2}$$

$$HCO_3^- + OH^- \rightleftharpoons CO_3^{2-} + HO_2, \tag{3}$$

$$Na^+ + HCO_3^- \rightarrow NaHCO_{3,(s)}. \tag{4}$$

When the product of Na^+ and HCO_3^- concentrations exceeds the solubility product (S), precipitation (reaction 4) occurs, resulting in the formation of a suspension (volumetric fraction of solid in the suspension at the outlet is 7–10%).

$NaHCO_3$ is used for various pharmaceutical (effervescent pills) and paramedical applications (hemodialysis), and in several industrial processes. Although the $NaHCO_3$ industrial process exists for more than 100 years, its operation

* Corresponding author. Tel.: +32-2-650-40-96; fax: +32-2-650-29-10.
E-mail address: bhaut@ulb.ac.be (B. Haut).

0009-2509/$ - see front matter © 2004 Elsevier Ltd. All rights reserved.
doi:10.1016/j.ces.2004.07.110

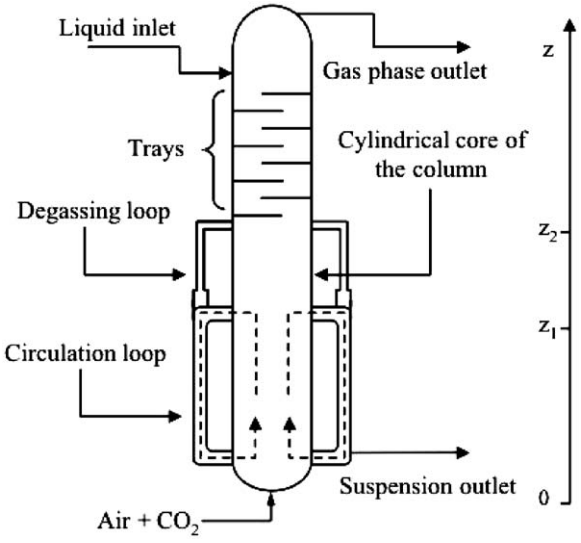

Fig. 1. Schematic representation of the column.

and optimization are still mostly empirical. There are today some limits to this approach for applications requiring high levels of purity and well-defined granulometry. Accordingly, Solvay is seeking for a more fundamental approach.

The model developed in this paper aims to serve this purpose. Its structure is derived from experimental studies on the industrial column and on a pilot column, also located in Dombasle. The balance equations are then generated. The resulting set of equations is not closed, as it contains too many unknowns. Its closure is performed from several experimental, bibliographical and Computational Fluid Dynamic (CFD) studies. A model of mass transfer between a bubble and a liquid is also developed. As some of the steps involved are fairly widely used, emphasis will be put on original aspects in the development of the model.

2. Model construction and balance equations

2.1. Liquid phase

The column is divided into a set of compartments placed in series. In each compartment, the liquid phase is distributed in two zones: a perfectly mixed bulk zone and a small zone near the gas–liquid interface with concentration gradients. The volume of the latter is negligible in comparison with the volume of the bulk zone. The first compartment ranges from the bottom of the column to the first tray. The tray region is divided into M compartments of identical height. Between two adjacent compartments, mass transfer of a dissolved species has two contributions. First contribution is the transfer induced by the flow rate Q. Second contribution is the transfer induced by a liquid back mixing flow rate Q_r. As shown later, tracing experiments validate the structure of this model.

Thermodynamic equilibrium is assumed for reactions (2) and (3) in the bulk zones of the liquid. The pH in the column is found from experimental data close to 10. It can therefore be shown that X mol of CO_2 added in the bulk zone of the liquid in a given compartment produce approximately $2X$ mol of HCO_3^- and $-X$ mol of CO_3^{2-} in this zone. Balance equations for HCO_3^- and CO_3^{2-} can therefore easily be written on the bulk zone of the liquid in each compartment. The rate of gas–liquid CO_2 transfer appears in these equations. Concentrations of the other dissolved species in the bulk zones of the liquid can be related to the concentrations in HCO_3^- and CO_3^{2-} through the equilibrium equations.

2.2. Solid phase

It is assumed that the solid phase is perfectly mixed for $z < z_1$ and absent for $z > z_1$. Crystal size distribution measurements performed on suspension samples at different locations in the column validate these assumptions. Sedimentation speeds of the solid are important (2 cm/s in average) and the solid phase can be found only in the zone where an air-lift motion is created by the circulation loops. It is also assumed that the solid and liquid phases are at thermodynamic equilibrium.

2.3. Gas phase

The industrial column is first characterized by measurements of pressure, suspension density and concentrations in liquid phase at different locations and for two operating points: at a low gas flow rate (2500 Nm^3/h) and at a high gas flow rate (4000 Nm^3/h). A global CO_2 transfer yield is computed from these measurements.

From measurements of pressure in the column, it can be shown that gas hold-up superior to 20% (and inferior to 40%) are likely to be met in the cylindrical core of the column. Therefore, the gaseous flow in the cylindrical core of the column is expected to be heterogeneous (coexistence of small and large bubbles), regardless of the operating point (Ellenberger and Krishna, 1994). Measurements of pressure and gas consumption also show that strong variations of the superficial gas velocity are expected within the cylindrical core of the column, at a given operating point. Following Ellenberger and Krishna (1994), small bubbles have an ellipsoidal shape and an equivalent diameter of 2–5 mm and large bubbles have the shape of a spherical cap and an equivalent diameter of 5–8 cm.

To model the impact of this complex flow pattern on the transport of CO_2 in the column, several simplifying assumptions have to be made.

First of all, gammametric measurements are performed on a classical bubble column with smaller dimensions than the industrial one (scale factor 1/4). It is filled with water at 25 °C and air is injected through a sparger or a cranted ring. No gas–liquid transfer occurs within the column.

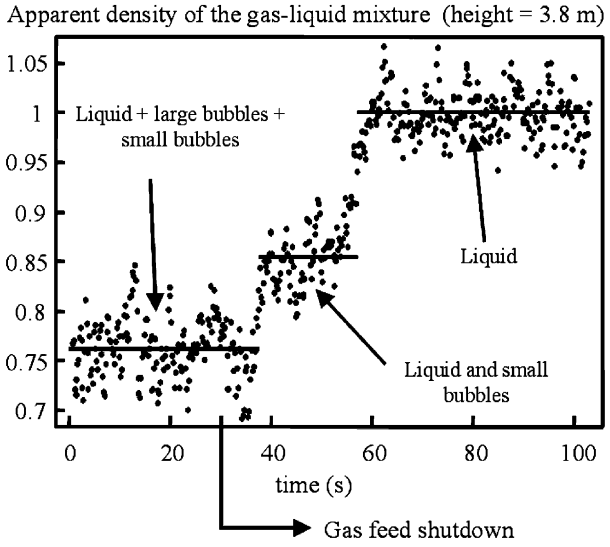

Fig. 2. Time evolution of the gas–liquid mixture density at a given height in the pilot column. Superficial gas velocity at the top is 17.6 cm/s. It roughly corresponds to the high gas flow rate of the industrial column. The sparger is used.

In the gammametric technique, the attenuation of a beam of gamma particles between a radioactive source and a receptor located at the same height on both sides of the column diameter (L) is measured. The Beer–Lambert law links the intensity of the emitting beam (I_0) and the intensity of the transmitting beam (I) as follows

$$\ln\left(\frac{I}{I_0}\right) = -\alpha L. \qquad \frac{dI}{dx} = -\alpha . I \tag{5}$$

It is assumed that α varies linearly with the apparent density of the gas–liquid mixture met by the beam. This variation is identified using only water and only air. The measurement of I and the knowledge of I_0 give α and therefore the apparent density of the gas–liquid mixture met by the beam.

Two types of experiments are performed. First of all, source and receptor are fixed at a given height. The column operates under steady-state conditions. Then, the gas feed is shut down and the average density of the water–air mixture met by the beam is measured as a function of time. An experimental result is presented in Fig. 2. This is just the reverse of the classical Dynamic Gas Disengagement Technique (Boyer et al., 2002).

Two sharp transitions are observed. First transition occurs when all the spherical caps located below the height of measurement at the time of the gas feed shutdown rise above this position. Similarly, second transition occurs when all the small bubbles located below the measurement height at the time of the gas feed shutdown rise above it.

This experiment clearly demonstrates the existence of two bubble populations. Four gas hold-up at the measurement height are calculated: the total gas hold-up (ε_t), the small bubble hold-up in the liquid–small bubble mixture (ε_d) and large and small bubble hold-up (ε_1 et ε_2). The results obtained are summarized in Table 1. It is observed that increasing the gas flow rate induces mainly an increase in large bubble hold-up.

Table 1
Results of the first gammametric experiments

	Sparger 17.6 cm/s	Cranted Ring 8.3 cm/s	Cranted Ring 17.6 cm/s
ε_d	0.146	0.139	0.144
ε_1	0.108	0.049	0.122
ε_2	0.130	0.133	0.127

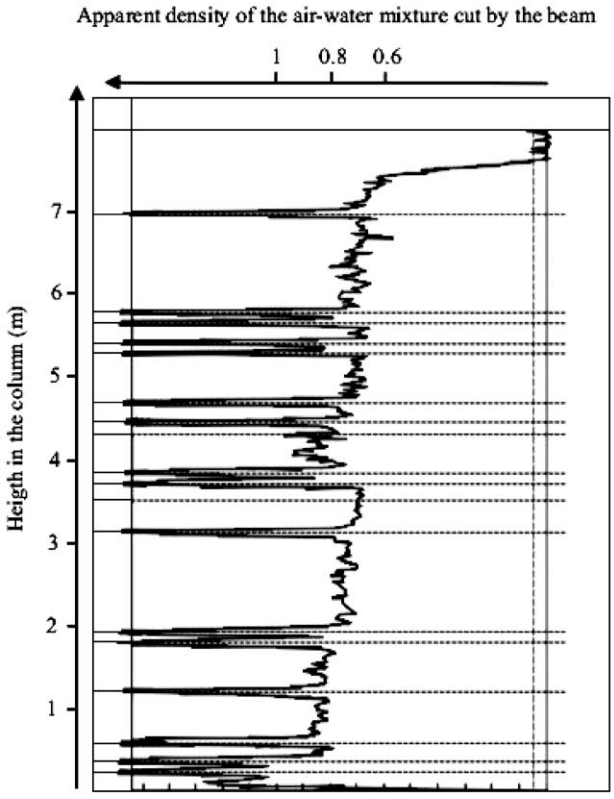

Fig. 3. Evolution of the apparent density as a function of the height of the column (cranted ring and superficial velocity of 17.6 cm/s at the top).

During the second set of experiments, the evolution of α as a function of the height in the column operating under steady-state conditions is measured. Fig. 3 shows the evolution of the apparent density of the gas–liquid mixture using the cranted ring and for a gas superficial velocity of 17.6 cm/s at the top of the column. As the liquid height at rest is 6 m, the corresponding gas superficial velocity at the bottom is 11 cm/s.

It is observed that the 6.6 cm/s variation of the gas superficial velocity between the top and the bottom of the column leads to a 10% variation in gas hold-up between the top and the bottom of the column (see Fig. 3). The small bubbles rise at a speed of about 20 cm/s, while the large bubbles rise at a speed of about 60 cm/s. Therefore, it seems that the increase of the gas superficial velocity between bottom and top of the

column essentially leads to an increase of the large bubble gas hold-up between bottom and top of the column, while the small bubble hold-up remains almost constant within the column. With $N_2(z)$ the molar flux of small bubbles at column height z, $dN_2/dz < 0$. The small bubble population transfers mass to the large bubble population.

In the model, each bubble population in the cylindrical core of the column is modeled as a plug flow reactor. It is considered that within the liquid—small bubble mixture, the volumetric fraction of the small bubbles ε_d is constant throughout the cylindrical core of the column but dependent of the operating point. This assumption is somewhat coherent with the observations of Ellenberger and Krishna (1994) and with the observations made during the gammametric measurements. It can be written

$$\varepsilon_2(z) = [1 - \varepsilon_1(z)]w[\varepsilon_d, \phi], \tag{6}$$

where

$$w[\phi, \varepsilon_d]^{-1} = 1 + \frac{1-\varepsilon_d}{\varepsilon_d}\,\frac{\rho_1\phi + \rho_c[1-\phi]}{\rho_c[1-\phi]}, \quad z < z_1, \tag{7}$$

$$w[\phi, \varepsilon_d] = \varepsilon_d, \quad z > z_1. \tag{8}$$

As z increases, the gas flux is dilated by the decrease of pressure and contracted by the transfer of CO_2 towards the liquid phase. As these two phenomena have no reason to compensate each other, the assumption of a constant ε_d in the cylindrical core of the column is likely to lead to a net mass exchange between the two bubble populations (as pointed out previously in the pilot column).

When $dN_2/dz + \varepsilon_2(z)T_2(z) < 0$, a net mass transfer from the small bubbles to the large ones takes place (through coalescence). The resulting transfer of CO_2 from the small to the large bubbles is given by $J(z) = -[dN_2/dz + \varepsilon_2(z)T_2(z)]y_2(z)$.

When $dN_2/dz + \varepsilon_2(z)T_2(z) > 0$, a net mass transfer from the large bubbles to the small ones occurs (through breakage). This situation is likely to occur at the bottom of the column where high pressure leads to an important transfer of CO_2 towards the liquid phase. The resulting transfer of CO_2 from the large to the small bubbles is $-J(z) = [dN_2/dz + \varepsilon_2(z)T_2(z)]y_1(z)$.

Each break-up and coalescence phenomenon leads to an exchange of CO_2 between the two bubble populations. Therefore, an exchange has to be superposed to $J(z)$. It is assumed that this exchange can be written $B\varepsilon_1(z)\varepsilon_2(z)[y_1(z) - y_2(z)]$. At a given operating point, the proportionality coefficient B is assumed constant throughout the column. Using the model, it can be shown a posteriori that this exchange is of significant importance.

The following equations are proposed to describe, together with Eq. (6), the transport of CO_2 in the cylindrical core of the column

$$N_1(z) = \frac{P(z)}{RT}\,\varepsilon_1(z)\left(G_1 + \frac{U_c(z)}{1-\varepsilon_1(z)-\varepsilon_2(z)}\right), \tag{9}$$

$$N_2(z) = \frac{P(z)}{RT}\,\varepsilon_2(z)\left(G_2 + \frac{U_c(z)}{1-\varepsilon_1(z)-\varepsilon_2(z)}\right), \tag{10}$$

$$\frac{dN}{dz} = -\varepsilon_1(z)T_1(z) - \varepsilon_2(z)T_2(z), \tag{11}$$

$$\frac{d}{dz}(N_2y_2) = -\varepsilon_2(z)T_2(z) - J(z) + B\varepsilon_1(z)\varepsilon_2(z)(y_1(z) - y_2(z)), \tag{12}$$

$$\frac{d}{dz}(N_1y_1) = -\varepsilon_1(z)T_1(z) + J(z) + B\varepsilon_1(z)\varepsilon_2(z)(y_2(z) - y_1(z)), \tag{13}$$

$$\frac{dP}{dz} = -\frac{\rho_c\rho_1}{\phi(\rho_1-\rho_c)+\rho_c} \times (1 - [\varepsilon_1(z) + \varepsilon_2(z)])g, \quad z < z_1, \tag{14}$$

$$\frac{dP}{dz} = -\rho_i(1 - [\varepsilon_1(z) + \varepsilon_2(z)])g, \quad z > z_1. \tag{15}$$

Eqs. (11)–(13) are singular at $z = z_1$, and $z = z_2$. It is assumed that $y_1(z)$ and $y_2(z)$ are continuous at $z = z_1$. It is equivalent to assume that $z = z_1$ is not a place where break-up and coalescence phenomena are privileged. At $z = z_1$, $N(z)$ is discontinuous: $N(z_1^+) = (1-f)N(z_1^-)$, where f is the fraction of the gas molar flux drifted in the degassing loops (Fig. 1, total degassing is assumed). The discontinuities of $N_1(z)$ and $N_2(z)$ can be derived from the discontinuity of $N(z)$, using Eqs. (6)–(8) and $N(z) = N_1(z) + N_2(z)$.

At $z = z_2$, the gas flowing through the degassing loops is reintroduced in the cylindrical core of the column. It is assumed that it generates large bubbles. Therefore, $y_2(z_2^+) = y_2(z_2^-)$ and $y_1(z_2^+)$ can be linked to $y_2(z_2^+)$ through a balance on the inert gas. At $z = z_2$, we have: $N(z_2^+) = N(z_2^-) + fN(z_1^-)$.

Finally, it is assumed that, at the level of each tray, coalescence phenomena are important enough to equalize the concentrations in CO_2 within the two bubble populations. This assumption leads to jump conditions for $y_1(z)$ and $y_2(z)$ at the level of each tray.

3. Closure of the model

3.1. Back mixing flow rate Q_r

The back mixing flow rate is identified as a function of the inlet gas flow rate applying least-squares optimization to tracing experiments performed on the industrial column. As different kinds of injection are performed at a given operating point, cross validations can be realized. Example of such a cross validation is given in Fig. 4.

3.2. Parameters G_1 and G_2

Using the Davies and Taylor equation (with a wake angle of 1 rad), it is assumed that $G_1 = 0.66(gd_1)^{1/2}$ (Clift et al., 1978, p. 205), where d_1, the equivalent diameter of the

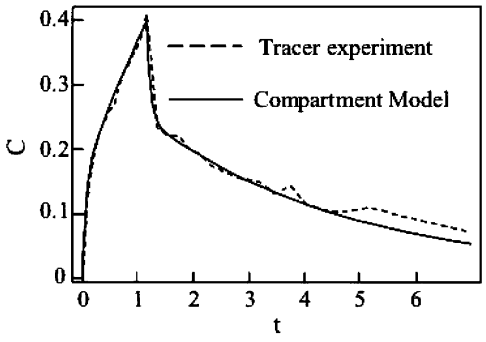

Fig. 4. Cross validation of the identified parameter Q_r.

large bubbles, is an adjustable parameter of the model. At a given operating point, it is assumed that d_1 is independent of z. This assumption of a single diameter d_1 independent of z describing the large bubble population is open to criticism but we do not have any reliable material to do better. However G_1 varies slowly with d_1. Similarly, it is assumed that the small bubble population can be described by a single equivalent diameter d_2, independent of z. It is equivalent to assume that the lifetime of a small bubble is smaller than the time it needs to undergo a significant diameter change under pressure variation or CO_2 consumption and that the newly generated small bubbles have all the same diameter.

Clift et al. (1978) proposes a correlation for the terminal velocity of a single ellipsoidal bubble in a liquid initially at rest. In the liquid of the column and for a bubble diameter in the interval 2–5 mm, the velocity given by this correlation is almost constant and its average is 0.185 m/s. In the model, it is assumed that $G_2 = 0.185\,\mathrm{m/s}$.

3.3. Gas–liquid mass transfer

Aim of this section is to derive and expression $T_j(\xi_i < z < \xi_{i+1}) = f([CO_2]_i, [OH^-]_i, d_j, P(z), y_j(z))$ where j states for 1 or 2 whether the transfer from large or small bubbles is considered.

Following Levich (1962), two small boundary layers where viscous effects play a significant role exist on both sides of the gas–liquid interface of a rising bubble. Within the boundary layer in the liquid phase and near the point of incidence (where $\theta = 0$, see Fig. 5), the transport of CO_2 is modeled by the following equation:

$$u_j \frac{\partial C_j}{\partial x} = D \frac{\partial^2 C_j}{\partial y^2} - k[OH^-]_i C_j, \tag{16}$$

where x and y are coordinates, respectively tangential and normal to the interface ($x = 0$ at the point of incidence and $y = 0$ at the interface). Following Hikita and Asai (1976), reaction (2) can be considered irreversible and of pseudo-first order at pH around 10.

Let a_j be the interfacial area active in the transfer of CO_2 of a bubble from population j, divided by the volume of the

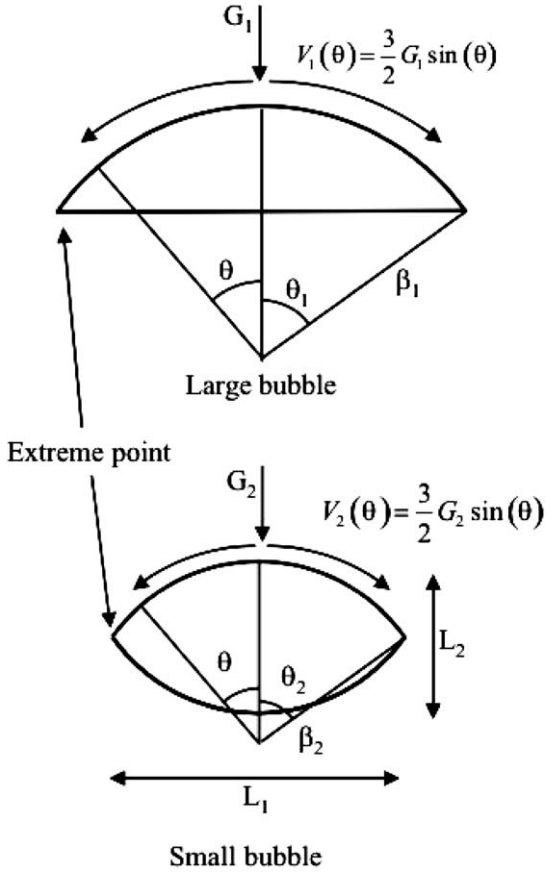

Fig. 5. Morphologies of small and large bubbles.

bubble. It is assumed that large bubbles are perfect spherical caps with a wake angle θ_1 (Fig. 5) of 1 rad. The radius of curvature β_1 (Fig. 5) of the large bubbles can therefore be related to d_1. It is assumed that the flat base of the spherical caps is inactive for the transfer of CO_2. a_1 can therefore be related to d_1.

It is assumed that the small bubbles are the superposition of two identical perfect spherical caps (Fig. 5). The ratio L_1/L_2 (Fig. 5) is identified as a function of d_2 using the correlation of Wellek (Clift et al., 1978). The wake angle θ_2 and β_2 (Fig. 5) are therefore identified as functions of d_2. a_2 is related to d_2 assuming that only the upper spherical cap is active for the mass transfer.

The Reynolds number of the bubbles in the column is larger than 10^3. Therefore, following Levich (1962), the flow in the liquid boundary layer does not differ significantly from the main flow that can be assumed inviscid. The flow of an inviscid liquid around a sphere rising at a velocity G can be computed analytically. The velocity magnitude at the liquid-sphere interface is $V(\theta) = 3/2G\ \sin(\theta)$. For the large bubbles, this solution is assumed to be valid for $0 < \theta < \theta_1$ (Fig. 5). u_1 is identified with the average of this velocity between 0 and θ_1: $u_1 = 3/2G_1(1-\cos(\theta_1))/\theta_1$. For the small bubbles, this solution is assumed to be valid for $0 < \theta < \theta_2$ (Fig. 5). u_2 is identified with the average of this velocity

between 0 and θ_2: $u_2 = 3/2G_2(1-\cos(\theta_2))/\theta_2$. Let $t_{c,j}$ be the contact time between a bubble from population j and a fluid element entering the liquid boundary layer at the point of incidence and leaving it at the extreme point (Fig. 5). It is assumed that

$$t_{c,1} = \frac{2\beta_1}{3G_1}\frac{\theta_1^2}{1-\cos(\theta_1)}, \quad t_{c,2} = \frac{2\beta_2}{3G_2}\frac{\theta_2^2}{1-\cos(\theta_2)}. \tag{17}$$

$T_j(z)$ is assumed to be given by

$$T_j(z) = -a_j\frac{D}{u_j t_{c,j}}\int_0^{u_j t_{c,j}} \left.\frac{\partial C_j}{\partial y}\right|_{x,y=0} \mathrm{d}x, \tag{18}$$

where $C_j(x, y)$ is the solution of Eq. (16) supplemented by adequate boundary conditions.

As D is several orders of magnitude smaller than the kinematic viscosity of the liquid, the liquid boundary layer can be seen as a semi-infinite medium with respect to CO_2 (Levich, 1962). Boundary conditions of Eq. (16) read

$$\lim_{y\to\infty} \left.\frac{\partial C_j}{\partial y}\right|_x = 0, \tag{19}$$

$$C_j(x, y=0) = HP(z)y_j(z), \tag{20}$$

$$C_j(x=0, y) = [\mathrm{CO_2}]_i. \tag{21}$$

Using Laplace transforms, it can be shown that the solution of Eq. (16) satisfying these boundary conditions is

$$C_j(x, y) = [\mathrm{CO_2}]_i \exp\left(-k_i^*\frac{x}{u_j}\right)\mathrm{Erf}\left(\frac{y}{2\sqrt{Dx/u_j}}\right) + HP(z)y_j(z)\frac{y}{2\sqrt{\pi D}} \times \int_0^{x/u_j}\frac{\exp(-k_i^*\lambda - y^2/4D\lambda)}{\lambda^{3/2}}\mathrm{d}\lambda. \tag{22}$$

To express $T_j(z)$, Eq. (22) has to be injected in Eq. (18). Unfortunately, some integrals in the resulting expression cannot be evaluated. A tractable expression for $T_j(z)$ can however be obtained. $\exp(-k_i^*\lambda)$ and $\exp(-k_i^* x/u_j)$ are replaced in Eq. (22) by a fourth-order polynomial in $k_i^*\lambda$ and $k_i^* x/u_j$. The coefficients of this polynomial are identified from least-squares optimization between 0 and 4. $k_i^* t_{c,j}$ is indeed inferior to 4 in the column. This can be checked a posteriori. After this substitution, the new expression for $C_j(x, y)$ is injected in Eq. (18). Some lengthy calculations lead to the following expression:

$$T_j(z) = a_j\sqrt{\frac{D}{t_{c,j}}}\left(\begin{array}{l} HP(z)y_j(z)\left[\sum_{p=0}^{4}\alpha_p(t_{c,j}k_i^*)^p\right] \\ -[\mathrm{CO_2}]_i\frac{\mathrm{Erf}[\sqrt{t_{c,j}k_i^*}]}{\sqrt{t_{c,j}k_i^*}}\end{array}\right), \tag{23}$$

where the α_p's are constants. They are evaluated once and for all.

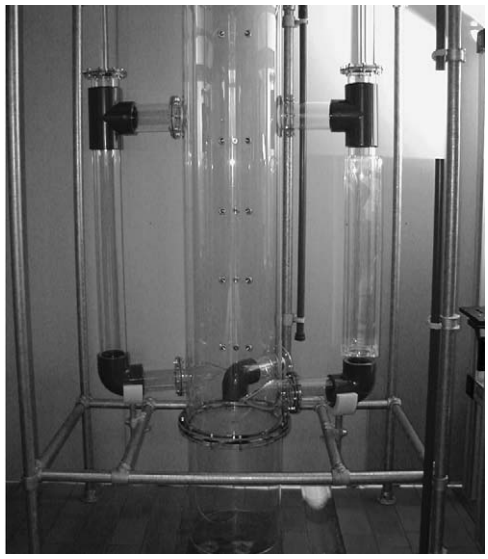

Fig. 6. Plexiglas copy of the lower part of the column.

3.4. Literature survey and data provided by Solvay

When solving the equations of the full model, the different physicochemical parameters appearing in these equations ($D, k, S, H, \ldots$) are allowed to vary with the operating temperature and the different $[A]_i$'s. These laws are mostly found in the literature (Vas Bhat et al., 2000). Concerning S and ρ_i, correlations are built from experimental data provided by Solvay.

3.5. Gas–liquid eulerian CFD simulations

Aim of the eulerian three phase (liquid, large bubbles and small bubbles) simulations is to identify f and $U_c(z)$ as functions of the operating gas flow rate. These simulations are realized in Fluent 6. The presence of the solid is neglected. The flow in the column is modeled for $z < z_2$. In this region, the properties of the liquid phase are uniform. The net exchange of matter between the populations and the transfer of CO_2 towards the liquid phase are neglected in the simulations. The gas is assumed incompressible. The 60×10^3 nodes mesh is generated in Gambit. The k-ε dispersed closure is applied for turbulence. Time steps of 5×10^{-3} s are used in the simulations. Steady state is reached after 1 week of computation on a Pentium 4 (1.4 GHz).

G_2 is set to 0.185 m/s. G_1 is set to 0.55 m/s. The ratio of the superficial velocities of the two bubble populations at $z = 0$ is adjusted such that a volume fraction of the small bubbles within the liquid—small bubble mixture of about 0.14 is reached.

A lab scale Plexiglas copy of the lower part of the industrial column is constructed using a scale factor 1/6 (Fig. 6). By means of Particle Image Velocimetry, liquid velocity fields in the circulation loops are measured for various superficial gas velocities. At a gas superficial

Table 2
Comparison between the model and data collected on the industrial column

	Measurements	Model
Molar fraction of CO_2 in the gas outlet	0.17	0.17
Pressure below the tray region (bars)	1.30 ± 0.05	1.37
Pressure at the bottom of the column (bars)	2.45 ± 0.04	2.46
Mass fraction of solid in the suspension outlet	0.18 ± 0.02	0.20
HCO_3^- concentration in the suspension outlet	1.54 ± 0.03	1.53
CO_3^{2-} concentration in the suspension outlet	0.28 ± 0.02	0.28

Low gas flow rate (2500 Nm^3/h). The concentrations are dimensionless. They are divided by their average values at the inlet (in mol/m^3). $d_1 = 7$ cm, $d_2 = 5$ mm, $\varepsilon_d = 0.13$ and $B = 10\,mol/(m^3\,s)$.

Table 3
Comparison between the model and data collected on the industrial column

	Measurements	Model
Molar fraction of CO_2 in the gas outlet	0.16	0.17
Pressure below the tray region (bars)	1.33 ± 0.03	1.37
Pressure at the bottom of the column (bars)	2.31 ± 0.05	2.24
Mass fraction of solid in the suspension outlet	0.18	0.20
HCO_3^- concentration in the suspension outlet	1.55 ± 0.02	1.49
CO_3^{2-} concentration in the suspension outlet	0.26 ± 0.01	0.28

High gas flow rate (4000 Nm^3/h). The concentrations are dimensionless. They are divided by their average values at the inlet (in mol/m^3). $d_1 = 7$ cm, $d_2 = 4$ mm, $\varepsilon_d = 0.15$ and $B = 20\,mol/(m^3\,s)$.

velocity of 6 cm/s, a liquid velocity in the circulation loops of 36 cm/s is measured. When a gas superficial velocity of 6 cm/s is chosen, the three phase eulerian CFD simulation of the Plexiglas copy gives a liquid velocity in the circulation loops equals to 30 cm/s. Therefore, CFD seems to be an efficient tool to predict this velocity. The simulations of the flow in the industrial column yield a liquid velocity in the circulation loops of about 90 cm/s.

3.6. Use of data collected on the industrial column

Once the different closures discussed previously have been injected in the balance equations derived in Section 2, four parameters have yet to be identified: d_1, d_2, B and ε_d.

These parameters could be identified through a comparison between the model and the data collected on the industrial column (see Section 2). Unfortunately, we do not have enough data to proceed to a rigorous identification, using a mathematical criterion.

However, we find that setting $d_1 = 7$ cm, $d_2 = 4$–5 mm, $\varepsilon_d = 0.13$–0.15 and $B = 10$–$20\,mol/(m^3\,s)$ allow a satisfying reproduction of the behavior of the column with the model (Tables 2 and 3).

$d_1 = 7$ cm, $d_2 = 4$–6 mm and $\varepsilon_d = 0.13$–0.15 seem physically acceptable (Ellenberger and Krishna, 1994). ε_d increases with an increase of the operating gas flow rate. It is coherent with the results of Ellenberger and Krishna (1994). d_2 decreases with an increase of the operating gas flow rate. B increases with an increase of the operating gas flow rate. These two facts are coherent with the model of Prince and Blanch (1990).

In a general way, it is impossible to give significant different values to the four unknown parameters and to conserve such a good general coherence.

4. Conclusion

Different tools and approaches are used to develop the model of the studied column. The structure of the model is constructed following the compartment approach. Within this approach, the reactor is divided into a set of interconnected elementary blocks. The balance equations of the model are then derived.

In order to identify a possible structure for this compartment model, several experimental studies are realized. Apart from gammametric measurements, experimental techniques used are classical. First gammametric measurements are encouraging. They allow an interesting characterization of the gas phase within a bubble column. They are however pretty expensive.

Modeling of the liquid phase within a bubble column following the compartment approach is a well-proven technique. Within the balance equations relative to the liquid phase, the back mixing flow rate Q_r is identified from data collected on the industrial column in Dombasle.

Modeling of the gas phase following the compartment approach is a bit trickier, mainly because of the heterogeneous nature of the gas flow. In the model, the gas phase is strongly idealized and numerous assumptions are made. According to the gammametric measurements, two bubble populations are considered. It is assumed that each bubble population can be described by a single diameter independent of the height within the column. It is also assumed that within the mixture liquid—small bubbles, the volume fraction of the small bubbles (ε_d) is constant within the entire column. This assumption is motivated by the results of the gammametric study. A coefficient B describing the intensity of the CO_2 exchange between the two bubble populations is finally introduced. The two diameters, B and ε_d are identified from measurements performed on the industrial bubble column.

Notation

a_j	interfacial area active for the transfer of CO_2 of a bubble from population j, divided by the volume of the bubble, m^{-1}
$[A]_i$	concentration of species A in the bulk zone of the liquid in the ith compartment, mol/m^3 of liquid
B	proportionality coefficient, see Eq. (12), $mol/(m^3\,s)$
C_j	concentration of CO_2 in the liquid boundary layer near the interface of a rising bubble from population j, mol/m^3

d_i equivalent diameter of bubbles from population i, m
D diffusion coefficient of CO_2 in the liquid of the column, m^2/s
f fraction of the gas molar flux drifted in the degassing loops
g gravity acceleration, m^2/s
G gas to liquid relative velocity of a bubble, m/s
G_i gas to liquid relative velocity of bubbles from population i, m/s
H Henry's coefficient for the CO_2, mol/(N m)
$J(z)$ transfer of CO_2 from small to large bubbles resulting from a net mass exchange between the two populations, $mol/(m^3\,s)$
k kinetic constant of the reaction $CO_{2,(l)} + OH^- \rightarrow HCO_3^-$, $m^3/(mol\,s)$
k_i^* $k[OH^-]_i$, s^{-1}
L pilot column external diameter, m
$N_1(z)$ molar flux of large bubbles in the cylindrical core of the column, $mol/(m^2\,s)$
$N_2(z)$ molar flux of small bubbles in the cylindrical core of the column, $mol/(m^2\,s)$
$N(z)$ $=N_1(z) + N_2(z)$, $mol/(m^2\,s)$
$P(z)$ pressure in the cylindrical core of the column, N/m^2
R ideal gas constant, N m/(mol K)
Q liquid inlet flow rate, kg/s
Q_r liquid back mixing flow rate, kg/s
S solubility product, mol^2/m^6
$t_{c,j}$ contact time between a liquid element and a bubble from population j, s
T temperature in the column, K
$T_i(z)$ transfer of CO_2 from the bubbles of population i towards the liquid phase, expressed in mol of CO_2 per second and per unit volume of population i, $mol/(m^3\,s)$
u_j component of the relative liquid–gas velocity in the boundary layer near the interface of a rising bubble (from population j) tangential to this interface, m/s
$U_c(z)$ Superficial velocity of the suspension (when $z < z_1$, the solid is assumed to follow perfectly the liquid) or the liquid (when $z > z_1$) in the cylindrical core of the column, m/s
x coordinate tangential to the interface of a bubble, m
y coordinate normal to the interface of a bubble, m
$y_i(z)$ molar fraction of CO_2 in bubbles from population i in the cylindrical core of the column
z vertical coordinate in the column, m

Greek letters

α calibration coefficient, m^{-1}
β_i radius of curvature of a bubble from population i near the point of incidence, m
$\varepsilon_i(z)$ volumetric fraction of bubbles from population i in the cylindrical core of the column
ε_d volumetric fraction of the small bubbles within the mixture small bubbles + liquid, in the cylindrical core of the column
θ angular position (Fig. 5), rad
θ_1 wake angle of the large bubbles, rad
θ_2 wake angle of the upper spherical cap constitutive of the small bubbles, rad
ξ_i starting z coordinate of compartment i (liquid phase), m
ρ_c volumetric mass of the solid,kg/m^3
ρ_i volumetric mass of the liquid in the bulk zone of the ith compartment, kg/m^3
ϕ mass fraction of solid in the suspension

Acknowledgements

F.N.R.S. (Belgian national fund for scientific research) fellow researcher Benoît Haut acknowledges the fund for its financial support.

References

Boyer, C., Duquenne, A.-M., Wild, G., 2002. Measuring techniques in gas–liquid and gas–liquid–solid reactors. Chemical Engineering Science 57, 3185–3215.

Clift, R., Grace, J.R., Weber, M.E., 1978. Bubbles, Drops and Particles, Academic Press, New York, NY.

Ellenberger, J., Krishna, R., 1994. A unified approach to the scale-up of gas–solid fluidized bed and gas–liquid bubble column reactor. Chemical Engineering Science 49, 5391–5412.

Hikita, S., Asai, S., 1976. Chemical Engineering Journal 11, 123–129.

Levich, V.G., 1962. Physicochemical Hydrodynamics, Prentice-Hall, Englewood Cliffs, NJ.

Prince, J.P., Blanch, H.W., 1990. Bubble coalescence and break-up in air-sparged bubble columns. A.I.Ch.E. Journal 36, 1485–1499.

Vas Bhat, R.D., Kuipers, J.A.M., Versteeg, G.F., 2000. Mass transfer with complex chemical reactions in gas–liquid systems: two-step reversible reactions with unit stoichiometric and kinetic orders. Chemical Engineering Journal 76, 127–152.